ELSEVIER

Contents lists available at ScienceDirect

Earth and Planetary Science Letters

www.elsevier.com/locate/epsl



Climate-driven stress changes and normal fault behavior in the Lake Malawi (Nyasa) Rift, East Africa



Liang Xue*, Robert Moucha, Christopher A. Scholz

Department of Earth and Environmental Sciences, Syracuse University, Syracuse, NY, USA

ARTICLE INFO

Article history:
Received 1 April 2022
Received in revised form 14 June 2022
Accepted 22 June 2022
Available online xxxx
Editor: R. Bendick

Keywords: Malawi Rift lake load slip rate border fault intrarift fault

ABSTRACT

Climate-triggered fluctuations of surface masses, including ice and water, can cause transient stress in the Earth's crust, further affecting the slip behavior of faults over different temporal and length scales. In particular, lakes developed within active continental rifts may modulate the stress states and slip rates of rift border faults and intrarift faults. Here, we utilize a numerical model in a case study of the Malawi (Nyasa) Rift to understand the response of faults to mass fluctuations on the Earth's surface. The water level of Lake Malawi rose 600 m over the last 150 kyr, and significantly influenced the stress state of faults in rift valley. We find that such water load fluctuations can exert 4.6 MPa normal stress on fault planes and produce a negative Coulomb stress (down to -2.0 MPa) on fault planes as well as a pronounced reduction of slip (\sim 2 m) on fault planes within the rift. Moreover, along-strike differences in fault geometries and their position relative to the center of the water column load resulted in variable along-strike stress and slip changes. These results suggest that lakes that develop within continental rifts play an important role in the evolution of extensional faulting. Our case study provides a basis for evaluating the relationship between climate-driven surface mass variations and the subsurface stress state of fault planes and associated seismic potentials.

© 2022 Elsevier B.V. All rights reserved.

1. Introduction

Loads applied on the Earth's surface exert a fundamental control on the strain accumulation on fault planes (e.g., Bettinelli et al., 2008; Hampel et al., 2010). Such surface loads include glacial ice, sedimentary basins, lakes and marginal seas, and tidal forcing, and may occur on different spatial and temporal scales, within an earthquake cycle (short term) or over multiple earthquake cycles (long-term). Most short-term observations are based on geodetic and/or hydrological modeling, presenting spatiotemporal correlations between periodic surface mass loading/unloading and fault activity (e.g., Borsa et al., 2014). Moreover, changes in surface mass loads can perturb the subsurface stress field and further promote or suppress earthquakes in the critically-stressed seismogenic zone (Bettinelli et al., 2008; Johnson et al., 2017; Xue et al., 2020).

The majority of studies of the long-term correlation between surface mass loading/unloading and stress state change and associated seismicity have focused on deglaciation control of faulting over glacial cycle time frames (Craig et al., 2016; Hampel et al., 2007, 2010) or over sedimentary filling cycles (Ballato et al.,

* Corresponding author. E-mail address: lxue07@syr.edu (L. Xue). 2019; Olive et al., 2014). For example, melting of the Weichselian ice sheet in northern Sweden produced fault scarps up to 15 m-high and paleoearthquakes with magnitudes as large as Mw = 8 (Mörner, 2005). The melting of the Yellowstone ice cap gave rise to an acceleration of strain accumulation on the Teton fault in Basin and Range Province (Hampel et al., 2007). Similarly, deglaciation triggered considerable slip on the pre-existing weak zones in the Swiss Alps (Ustaszewski and Pfiffner, 2008). Beyond the glacial cycle, the effect of loading/unloading of climate driven lake storage on faulting has not been fully recognized or analyzed. Numerical experiments and field studies on long-term climate driven lake loading-derived stress changes in continental rift settings are seldom even reported.

The Malawi (Nyasa) Rift, with its active faulting and record of pronounced Quaternary climate variability, provides an ideal site to study long-term, surface mass redistribution-derived stress and slip rate changes on fault planes. The Malawi Rift is located at the southern end of the Western Branch of the East African Rift (EAR) (Fig. 1). Lake Malawi, the world's fourth largest lake by volume (Messager et al., 2016), is \sim 550 km long, \sim 700 m deep and covers the rift valley, with lake coastlines defined by major border faults. Its lake levels fluctuated dramatically over the last 150 kyr (Scholz et al., 2007; Lyons et al., 2015), rendering considerable variations

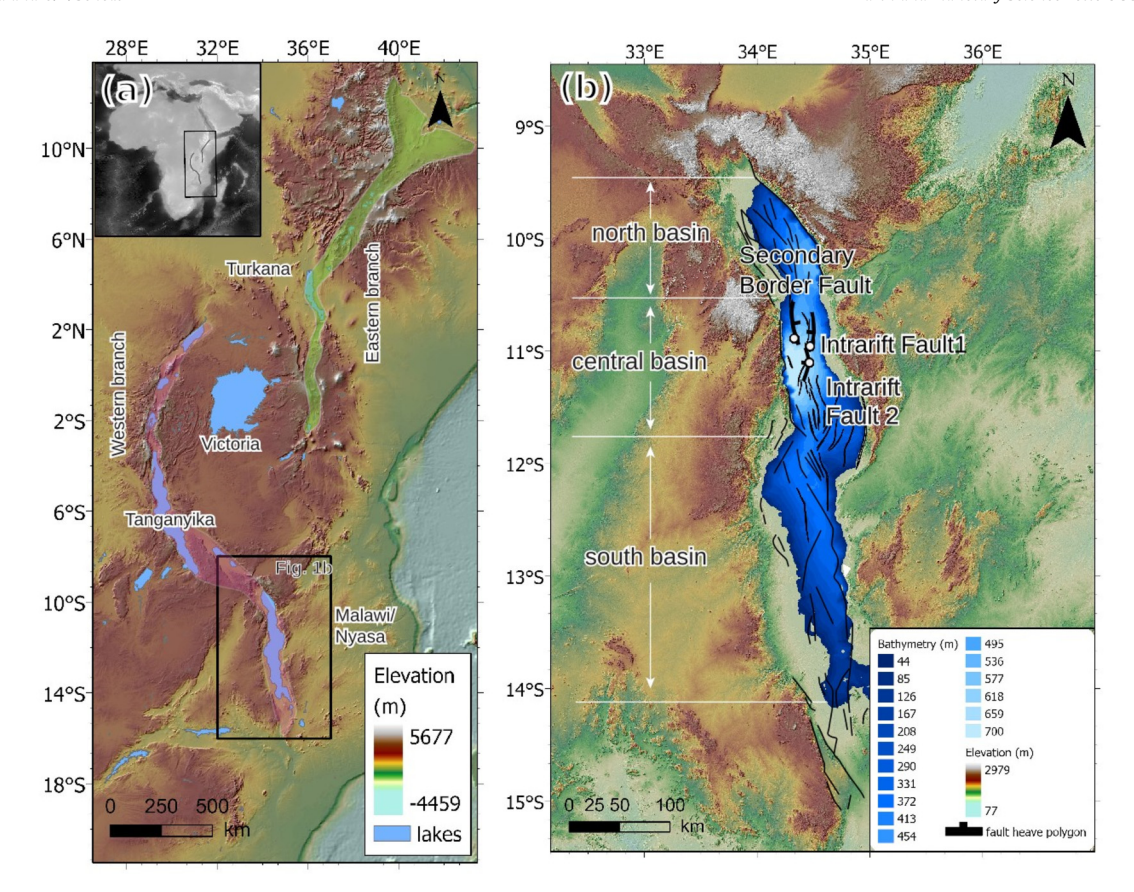


Fig. 1. (a) Topography of the East African Rift (EAR) with red and green shading illustrating the Western Branch and Eastern Branch, respectively. Major lakes along the EAR, including Turkana, Tanganyika, Victoria, and Malawi/Nyasa, are highlighted. The inset image shows the extent of Fig. 1a in Africa. The black box in the inset image defines the region of Fig. 1a. The black inset box in Fig. 1a defines the region of Fig. 1b. (b). Digital elevation model and bathymetry of the Lake Malawi region. The white circles and solid lines are locations of a secondary border fault (SBF) and intrarift fault 1 and 2 (IF1, IF2) studied in this work. The fault geometry and bathymetry are from previous work and active database (Scholz et al., 2007; Lyons et al., 2011; Scholz et al., 2020; Williams et al., 2021).

in mass loading. High-resolution sedimentary records of climate are available for the last 1.3 million years, and fault geometries are also well-constrained by subsurface imaging data sets (Lyons et al., 2015; Shillington et al., 2020; Scholz et al., 2020), allowing for quantification of the time-dependent surface loads from the lake water column.

To further understand the interactions between climate driven changes in surface mass loads and fault stress/slip rates, we focus on faulting in the Central Basin of Malawi Rift, the deepest basin in the rift lake (Figs. 1a and 1b), and present a suite of numerical experiments by using finite element code Pylith 2.2 (Aagaard et al., 2013) to evaluate the lake water load-derived stress and slip on fault planes. The objectives of this work include 1) determining the magnitude and timing of climate-driven lake loading in the Malawi rift over the past 150 kyr; 2) quantifying the stress and slip generated by the lake level fluctuations; and 3) determining if the fault geometry/location relative to the loading source could generate along-strike variations in stress and slip. This case study introduces the mechanisms of loading/unloading-related normal faulting and provides a basis for evaluating the relationship between climate-driven surface mass variation and subsurface stress on fault planes and their associated seismic potentials over a 150 kyr time frame. This stress state of fault planes can help to explain the heterogeneities of orientation, continuity, and strength of faults during continental extension. Our study suggests that surface mass changes driven by climate may modulate the spatiotemporal patterns of faulting, and the roles of lakes that developed within the continental rifts cannot be neglected during the evolution of extensional faulting.

2. Background

2.1. Tectonic background

The EAR is a part of seismically and volcanically active divergent plate boundary separating the Somalian, Nubian plates, and forming a series of microplates (Saria et al., 2014: Stamps et al., 2008; Wedmore et al., 2021; Fig. 1a). The EAR is composed of Eastern and Western Branches which generally follow Proterozoic mobile belts. With the evolution of the EAR, a 4000 km-long chain of rift basins and associated rift lakes developed from Ethiopia to Malawi. The Malawi Rift (Fig. 1b) is magma-poor, with large magnitude, deep earthquakes of long recurrence intervals (e.g., Albaric et al., 2009). Extension rates at the Malawi rift are slow, measuring 1-3 mm/yr (Saria et al., 2014; Stamps et al., 2018). The Lake Malawi section of rift valley is comprised of three extensional segments, as linked half-grabens (North, Central, and South Malawi; e.g., Ebinger et al., 1987; Scholz et al., 2020). Intrarift faults in the rift basin contribute \sim 20–25% and \sim 55% to the total extension of the northern and southern Malawi rift respectively (Shillington et al., 2020). The localization of fault development and geometry in North and Central Malawi may be influenced by the preexisting basement shear zones (Kolawole et al., 2018; Laó-Dávila et al., 2015; Njinju et al., 2019). Normal faulting is the dominant kinematic behavior, but strike-slip faults are also observed in the region (e.g., Delvaux and Barth, 2010). Fault throws on border faults exceed 8 km in some localities, and throws on intrarift faults as large as 6 km are also observed (Shillington et al., 2020). This extension-related subsidence and a favorable hydroclimate give rise to a deep lake with a maximum depth of 700 m. The lake

coastlines are commonly controlled by major border faults, and the lake's deepest point is near the west-central area of the Central Basin rift segment (Fig. 1b).

2.2. Background of climate and hydrology

As Lake Malawi is located in the tropics, the seasonal climate is controlled by changes in precipitation on account of north-south migration of the tropical rain belt or the Inter-Tropical Convergence Zone (ITCZ). Moisture is derived from both the Atlantic and Indian Oceans in a monsoonal circulation, forming a wet season from December to April (Lyons et al., 2011). Precipitation within the Malawi rift varies along-axis, where the southeast receives 800 mm/yr, but the north more than 2000 mm/yr (McSweeney et al., 2014). The variability is controlled by elevation and prevailing wind direction during the wet season (Lyons et al., 2011). Multiple large river systems (e.g. Rukuru, Bua, Ruhuhu, Songwe) discharge 70% of total inputs to the lake, and most enter the lake from the west. The Shire River in the south basin is the lake's only outlet (Bootsma and Hecky, 1999). Evaporation comprises 90% of the annual water loss of the modern lake, resulting in a highly sensitive water balance (Drayton, 1984).

Long-term climate of Lake Malawi region changed from a highly variable, orbitally-paced condition punctuated by megadroughts, to more humid conditions after \sim 70 kyr, possibly induced on account of reduced eccentricity (Scholz et al., 2007). The interval between 150 and \sim 70 kyr is dominated by periods of extreme drought conditions due to the peak of orbital eccentricity, and after that, the precessional forcing is weak during intervals of low eccentricity (Scholz et al., 2011). Climate models suggest that the southward shift of the austral summer Hadley cell can also provide an increase in latitudinal temperature gradient, leading to a rise of precipitation in the southern hemisphere, including Lake Malawi (Clement et al., 2004). Accordingly, this produced a long-term lake level transgression of Lake Malawi, as well as other lakes in the EAR over the past \sim 150 kyr. In the equatorial and northern hemisphere tropics of eastern Africa, high latitude northern hemisphere glacial conditions seem to also impact regional hydroclimate, resulting in drier conditions during peak glacial periods (e.g. Tierney et al., 2008).

3. Numerical model setup

To evaluate the behavior of a normal fault during lake water storage fluctuations, we designed a 350 km \times 700 km \times 200 km finite element model using PyLith v2.2.2 (Fig. 2) (Aagaard et al., 2013). The model domain incorporates three normal faults (one secondary border fault, two intrarift faults shown in Fig. 1b, here referred as SBF, IF1, and IF2, respectively) in the Central Basin, and the geometry of the studied faults is derived from seismic reflection data (Scholz et al., 2020). The depths of the three modeled faults are \sim 8 km based on available seismic data (Scholz et al., 2020). Note, the border fault here is not the primary border fault forming the coastline of the central basin but refers to an east-dipping secondary border fault situated on the outboard side of a relay ramp (Fig. 1b). This fault is chosen as the seismic reflection data image both the hanging wall and footwall of the fault.

Here, PyLith applies the conventional finite element formulation with a domain decomposition approach to implement fault slip. For each vertex along the negative side of a fault interface, a second vertex on the positive side of the fault and a vertex corresponding to the Lagrange multiplier is introduced. The elastic properties of the rheologically-layered crust are from a homogeneous 1-D model, the Preliminary Reference Earth Model (PREM, Dziewonski and Anderson, 1981). The crust thickness in the model is derived from recent receiver function study of Malawi Rift (Sun

et al., 2021). Our choice of viscosity properties is shown as Figs. S1, S2, and Table S1. We assign a pressure equivalent to the local water depth of Lake Malawi and add it on the surface of the domain as a Neumann boundary condition. For the other lateral and bottom boundaries, we fix the degrees of freedom of the direction of perpendicular the boundary to resolve the stress on fault planes. The temporal and spatial change of the loads are constrained by previously published lake level information from 150 kyr BP to present (Lyons et al., 2015), and by lake bathymetry data, respectively. The lake level is reconstructed by calibration of first principal component from geochemical and sedimentological variables directly influenced by lake-level variations and known lake levels (Lyons et al., 2015). The cell size of domain is \sim 1.5 km near the faults and increases to \sim 30 km towards the bottom model boundaries (Fig. 2). To evaluate the slip rate changes from surface loads, a constant background extension rate of 2.5 mm/yr (Saria et la., 2014; Stamps et al., 2008) is applied at the east and west side of the domain as a Dirichlet boundary condition. We note here, that a recent kinematic model using GNSS measurements yields a lower local extension velocity of 1.2 mm/yr across the southern Malawi Rift, indicating an elastic strain accumulation (Wedmore et al., 2021). Therefore, we include the simulation with boundary condition of a lower extension rate in the supplementary materials (Fig. S3). The induced slip rate is thus calculated at the different locations along the strike of fault for domains with only background extension, and with both extension and a lake load.

We simulate dynamic rupture scenarios in the PyLith code (Aagaard et al., 2013) to govern the fault stress and the slip using a static friction law, producing a shear traction proportional the fault normal traction (lake load) plus a cohesive stress:

$$\tau_{s} = \left\{ \begin{array}{l} T_{c} + \mu \sigma_{n}, \sigma_{n} \leqslant 0 \\ 0, \sigma_{n} > 0 \end{array} \right\}$$

Where τs is static shear stress, Tc is the cohesive stress, σn is the normal stress, and μ is coefficient of friction (e.g., Aagaard et al., 2013). When the friction is large enough, no sliding occurs, then the Lagrange multipliers correspond to the forces that keep the slip zero. When the driving forces exceed the friction, the Lagrange multipliers are reduced to be consistent with friction from the fault model. Here we apply $\mu=0.4$, as widely tested and applied in calculations of Coulomb stress changes to minimize uncertainty (e.g., King et al., 1994). Since it is not possible to predict the cohesive stress for potential rupture in this region, we assume a 1.0 MPa of cohesive strength excess in the static friction based on previous modeling efforts (Aagaard et al., 2013, 2017; Andrews, 2005). Therefore, slip could occur on fault plane where the lake water load derived static shear traction is more than 1.0 MPa.

We calculate the Coulomb stress for each of the studied fault planes. Coulomb stress is defined as $\Delta \text{CFS} = \Delta \tau 1 - \mu \Delta \sigma n$, where $\Delta \tau 1$ is the loading induced shear stress change (here and after refer as "shear stress"), and $\Delta \sigma n$ static normal stress change (e.g., King et al., 1994). Here, the pore fluid pressure is not considered in the Coulomb stress calculation, but would be evaluated in the discussion. We note that a positive Coulomb stress change implies that normal faulting is promoted, whereas a negative Coulomb stress change means that normal faulting is suppressed.

4. Results

4.1. Surface load changes over the past 150 kyr

The level of Lake Malawi fluctuated ~ 600 m over the last 150 kyr (Fig. 3), and from bathymetry and lake level data, we estimate that the water storage increased from its minimum 150 kyr ago by

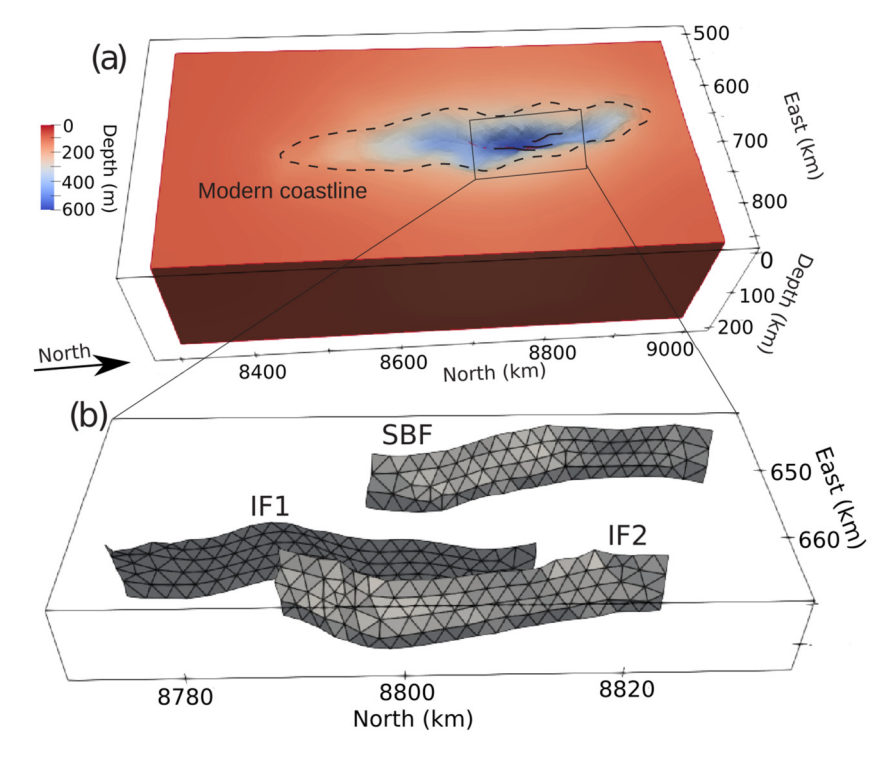


Fig. 2. (a) Domain of finite element model with a dimension of 350 km \times 700 km. The lake water load is added on the domain surface. The modern coastline of Lake Malawi is shown as a dashed line. (b) The three fault planes investigated in the Central Basin of Malawi rift are in the mesh. The geometry of the fault planes is derived from analysis of seismic reflection data sets (Scholz et al., 2020). The lake water storage fluctuation induced stress and slip rate is calculated on each node on the fault planes.

 \sim 5 Gigatons since 150 kyr BP (Fig. 3). This increase in water storage has resulted in an increase in surface loading on the Malawi Rift and associated fault planes. Notably, the North, Central, and South Basins experience lake loads different from each other, in magnitude and direction due to their dissimilar basin morphologies. Specifically, the Central Basin has been under a continuous water load since 150 kyr BP (Fig. 3), but such loads were absent in the North and South Basin for more than 50 kyr of the past 150 kyr due to their shallower configurations (Fig. 3). Likewise, the magnitudes of loads in the North and Central Basins are markedly larger than that of South Basin due to the shallower lake depth in the south (Figs. 1 and 3).

4.2. Surface load fluctuation-induced stress changes

The lake storage fluctuation-derived stress changes vary in amplitude and direction on each of the fault planes. The normal and shear stresses increase when the lake level increases from 150 kyr BP to present (Fig. 4). The normal stress change on three fault planes is consistent, where water level increase causes a compressional normal stress on the fault plane of 1.0-4.6 MPa (Figs. 4cg). However, the shear stress displays a different pattern; the increase of lake level gives rise to a dip-direction traction of 0.9 MPa on the modeled fault planes. Furthermore, the strike-slip shear stress on the fault planes is one order of magnitude lower than that of normal stress (Figs. 4ac). Lastly, the increased lake water load exerts a negative Coulomb stress on fault planes, and this negative stress changes from -0.5 MPa to -2 MPa from 150 kyr BP to present (Fig. 4). This reduced Coulomb stress on fault planes implies that the increase of lake level (increasing lake depth and loads) discourages normal faulting on all three faults beneath the lake. In PyLith the fault is represented by two groups fault nodes, which share the same nodes on the edges of the buried faults. These nodes on the edge are forced to slip to zero along the buried edges on the fault planes to ensure the continuity and coherence of the mesh (Fig. 4).

Our size of fault planes with cell of 1.5 km are sufficiently large to minimize this edge effect of the buried edges.

4.3. Along strike variation on induced stress/slip rate change

Within a single fault plane, the stress and slip patterns also exhibit large variations along strike. For example, the normal stress and dip-slip shear stress shows an increase from south to north of 1.5-2.0 MPa and 0.5 MPa on the SBF, respectively (Fig. 4). We further investigate the stress time series at different locations on fault planes (north, central, and south tips of the fault plane, location shown in Fig. 5a). Fig. 5 and Fig. 6 present the Coulomb stress and slip variations of the SBF and IF1 along the fault strike, respectively, and we also plot the slip with extension only, as a comparison to that with surface loading in Fig. 6. Notably, the phase of Coulomb stress throughout of the SBF and IF1 is constant, but the northern tip presents a higher magnitude (~2 MPa) of Coulomb stress than that of southern tip for both SBF and IF with the lake level rise (Fig. 5). For the slip rate changes, if only applying an extension rate of 2.5 mm/year without lake load, the accumulated slip would be 6-8 m on SBF and IF (dashed lines in Fig. 6). Such slip is reduced by adding lake water loads on the surface of the model, where the load would reduce the slip on both the SBF and IF, but to different degrees. The north tips of both SBF and IF especially are more sensitive to surface loads, showing a reduction of slip of 2-4 m over 150 kyr (Fig. 6); however the slip rate on the southern tip of the IF is only reduced by \sim 1 m (Fig. 6b). If applying a lower local extensional velocity (Wedmore et al., 2021), the reduction of slip would be 1-2 m over 150 kyr, showing decrease of 30-40% (Fig. S3). Furthermore, higher lake level since 100 kyr BP would significantly decelerate the slip on the north tip (green lines in Fig. 6) where the deepest lake is preserved. In contrast, when the lake level is low (e.g. 150-100 kyr BP), the faults show a rapid increase in their slip rate (Fig. 6). This observation agrees with the model stress state, where the increase of lake level would increase

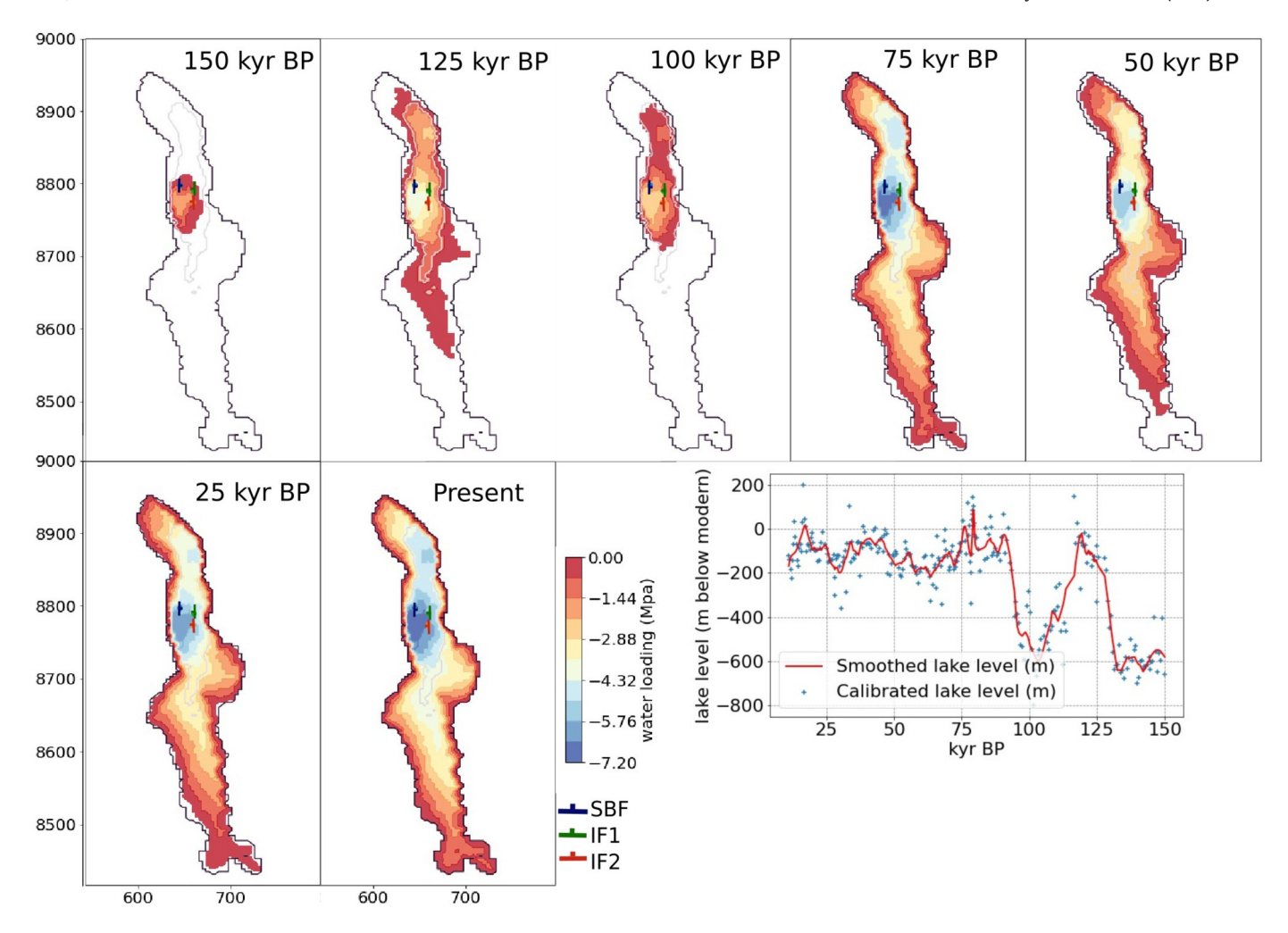


Fig. 3. The lake water derived loads from 150 kyr BP to present. The black contour shows the present coastline of Lake Malawi, the three color-coded lines represent the locations of the SBF, IF1, and IF2. The surface load from lake water storage is color coded. The inset plot shows the lake level fluctuation from 150 kyr BP to present from Lyons et al. (2015) with the plus marker and line represent the calibrated and smoothed lake level respectively.

the normal stress and thus decrease Coulomb stress to discourage fault rupture.

5. Discussion

Modeled results indicate that climate-driven rift lake storage fluctuations are able to cause considerable stress changes on rift basin normal faults. The increase of water levels in Lake Malawi since 150 kyr suppresses fault rupture of the rift. In turn, reductions in lake levels, which occurred periodically over a long-term lake level rise, increased Coulomb stresses on the rift basin normal faults. The Coulomb stress change in this setting is dominated by the normal stress. Thus, a rise in water level would increase the compressional normal stress and thereby clamp the fault. Although the lake level rise would also lead to shear stress increases which would promote failure, the normal stress change is one order of magnitude higher than that of shear stress during lake level rise from 150 kyr BP to present (Fig. 4). This triggering mechanism, as well as the correlation between surface mass removal and seismicity rate increase, has been reported in previous numerical experiments and field studies focused on glacial retreat. For example, Wu and Hasegawa (1996) found that faulting rates are increased considerably by postglacial unloading in parts of Canada based on a finite element technique. In parts of Scandinavia and North America, paleoseismologic evidence and field data suggested that melting of ice sheets was followed by reactivation of normal faults (Hampel and Hetzel, 2006). In Fennoscandia, a tectonically stable continental lithosphere, regional deglaciation is coincident with rise of seismicity (Craig et al., 2016). All these observations support the hypothesis that surface mass loading on normal faults can reduce the faulting and deter rupture affecting earthquake rates. In addition to the stress state of the fault plane, the slip rate is also under the influence of lake loads and the modeled slip rate history correlates with the stress change, where the slip is reduced by the increase of lake level from 150 kyr BP to present (Fig. 6). The ensemble of previous studies and our present work leads to the robust conclusion that surface mass loading, manifested as a 600 m lake level rise, is sufficient to reduce faulting beneath the lake.

Our results also suggest that transgression and regression of Lake Malawi can have a considerable effect on upper crustal deformation by modulating the slip rate and the stress state of adjacent faults. These faults were found to respond to loading by slip deceleration/Coulomb stress decrease, and to unloading by slip acceleration/Coulomb stress increase. Many major faults exhibit a cyclic release of elastic strain energy, as shown in multiple earthquake recurrence models globally (e.g., Thatcher, 1984). Beyond the earthquake cycles, glacial-interglacial changes could also modulate fault slip evolution and associated recurrence rates (e.g., Hampel et al., 2010). At the same time, climate-driven sedimentary loading and unloading cycles, which also modulate sedimentary fills and fluvial incision, can also control spatiotemporal deformation

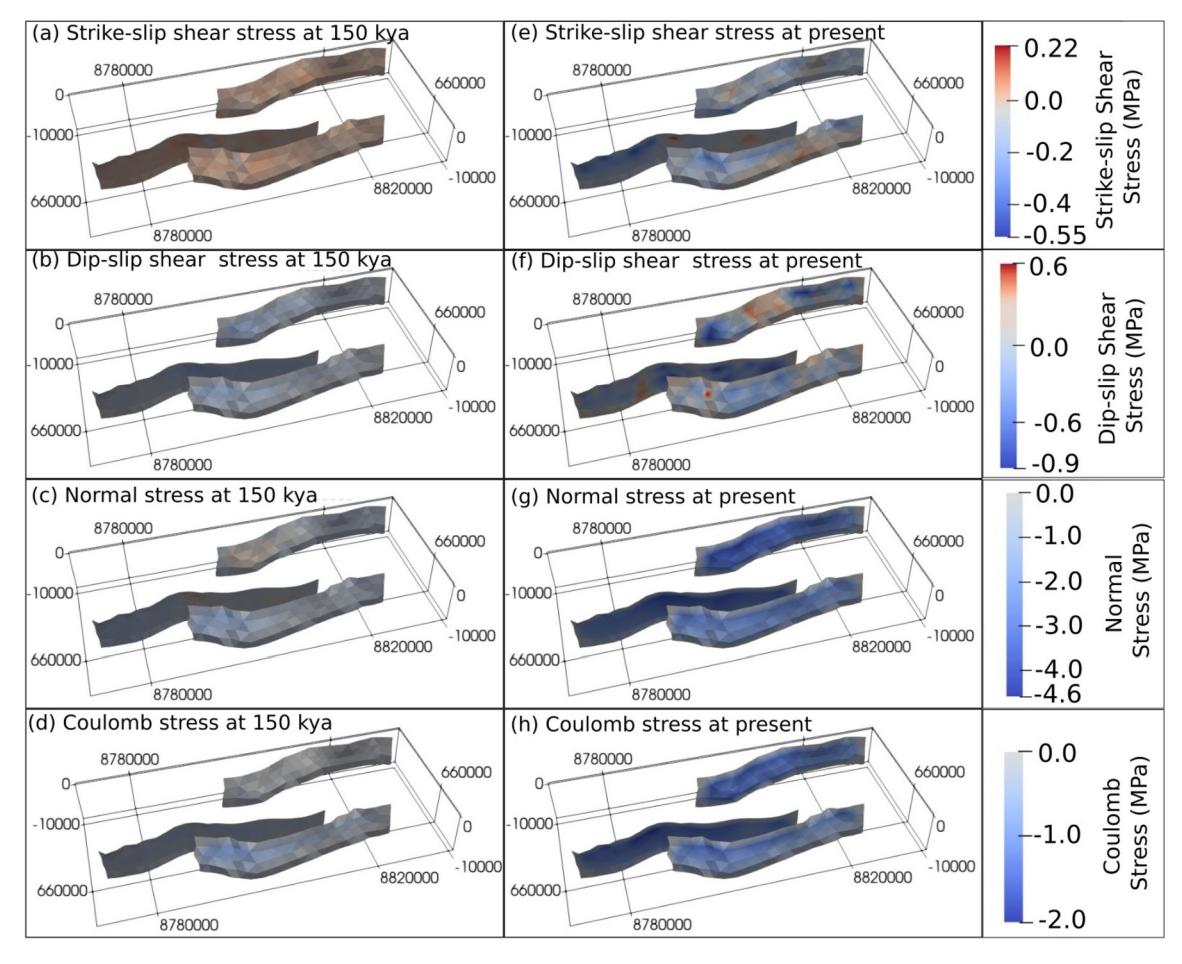


Fig. 4. Lake water load derived stresses on the three fault planes at 150 kyr BP (left column) and present (right column), illustrating strike-slip shear stress (ae), and dip-slip shear stress (bf), normal stress (cg), and Coulomb stress (dh) caused by a lake level increase of \sim 600 m in the Malawi Lake. The positive and negative strike-slip shear stresses represent left lateral and right lateral directions respectively. The positive and negative dip-slip shear stresses represent reverse and normal directions along-dip, respectively. The negative normal stress suggests compressional conditions.

of basins and faulting within it (e.g., Ballato et al., 2019; Olive et al., 2014). Similar to surface loads from lake water, 2D numerical experiments suggest that thicker sedimentary fills could suppress basinal faulting process, and removal of sedimentary loads promotes intrabasinal faulting (e.g., Ballato et al., 2019; Calais et al., 2010). Accordingly, there is abundant evidence that cyclic climate changes driving surface mass fluctuations can affect the accelerated or decelerated motion of faults. It is essential to investigate continental climate archives and reconstruct the Quaternary loading history to fully understand the strain release pattern of seismogenic faults and to further assess seismic hazards (e.g., Hodge et al., 2020). We suggest that the interplay between tectonics and climate, which dictate the transient storage of lake water and modulated loading stress, may occur in other continental rift lakes as well. These rift lakes in tropical Africa (e.g. Tanganyika and Malawi) experienced major and rapid hydrological fluctuations during the Late Pleistocene and Holocene and resulted in dramatic shifts between relatively moist and arid conditions. Reconstructions of paleoclimate could play an important role in deciphering the slip history and evolution of the EAR.

Notably, the magnitude of lake level fluctuation-induced Coulomb stress and slip reduction are relatively small compared to estimates of coseismic deformation. Our modeling results represent the minimum stress buildup and slip accumulation over multiple seismic cycles rather than coseismic instantaneous displacement, and are comparable to results obtained from modeling studies of different regions. For example, numerical modeling of

northern Scandinavia and Basin-and Range Province constrained by paleoseimic data concluded that unloading due to mass loss from a glacier (500 m of an ice sheet, similar to our lake level changes) could give rise to a differential stress of \sim 3 MPa and \sim 2 m fault slip (Hampel et al., 2010). Similarly, Steer et al. (2014) found that rapid erosion in Taiwan (20 mm/yr) can also result in Coulomb stress change of 0.01–0.1 MPa over the interseismic phase (500 yr). Furthermore, results from finite-element modeling of deglaciation of the Teton Range suggested \sim 5 m slip reduction from the unloading of Teton glaciers and Yellowstone ice cap (Hampel et al., 2007). To further reconcile the climate effects on stress/slip history of Malawi rift, paleoseismological studies and better age constraints are required.

Specific fault geometries, roughness, and position relative to the surface loads also impact the magnitude and directionality of stress buildup and slip rates on fault planes. We observe that along-strike variations of slip exist in cases with extension only (dashed lines in Fig. 6), and the surface loads accelerate the effect of fault geometry on fault planes. With lake loads, the first-order along-strike variation indicates a northward increase of stress and slip (Figs. 4 and 5). This is largely because the northern tips of these faults are closer to the maximum of water column load in the Central Basin. Besides, given that the strikes and dips of normal faults vary for different segments, the induced stress/slip on the fault planes also changes accordingly. For the SBF and IF1, their strike changes $\sim 12^\circ$ (Fig. 2b). The strike-slip shear stress changes from left-lateral to right lateral shear either side of the fault bend

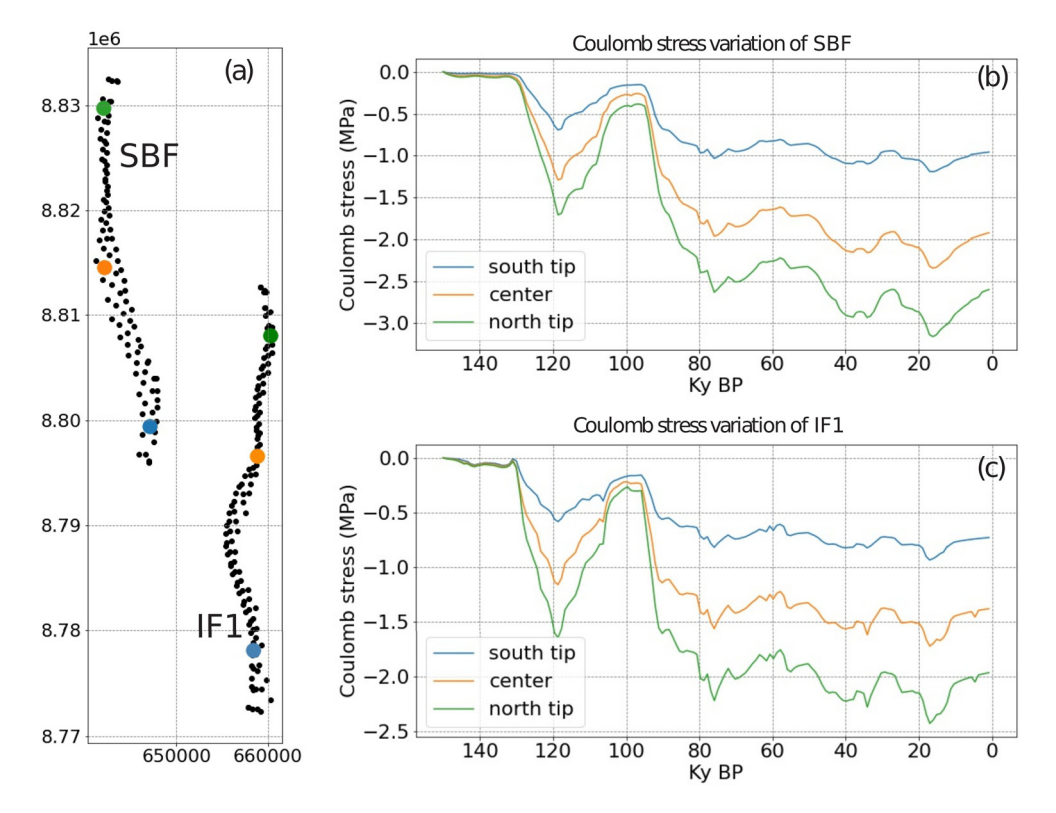


Fig. 5. Coulomb stress variations along the strike of SBF (b) and IF (c). The locations of selected cells on the fault are shown in (a). Each of the black dots represents a node on the fault plane. The x and y axes are in the units of meters in the UTM S36. Three nodes on the fault planes are chosen to show the stress time series, where the blue, orange, and green ones represent north, center, and south tips of the fault, to illustrate stress variations along fault strike.

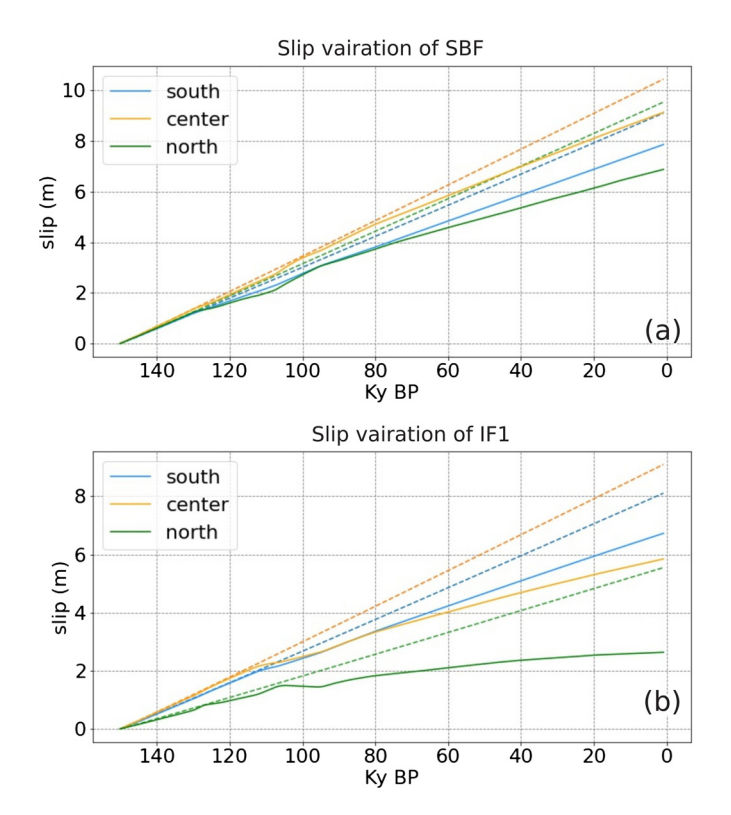


Fig. 6. Slip variations on (a) SBF and (b) IF1 at three observation points (north, center, and south of the fault). The dashed lines represent the modeled slip with an extension rate of 2.5 mm/year. The solid lines represent modeled slip with extension rate of 2.5 mm/year and lake load variations since 150 kyr BP.

(Fig. 4). Moreover, the normal stress and dip-slip shear stress also increase either side of this fault bend (Fig. 4).

To evaluate the effect of fault geometry, we compare the induced stress on the actual fault plane and on a simplified rectangular fault plane, where along-strike variations are removed (Fig. S4). The equation of this rectangular fault plane is calculated using the best fit of all the vertices on the actual fault plane (Fig. S4a). Figs. S4 show that the magnitude of induced normal stress on the best fit rectangular plane and actual plane are in the same order of magnitude; nevertheless, the pattern and magnitude of induced shear stress is different between best-fit rectangular plane and actual plane, where the shear stress changes with orientation of the fault planes but such variation is absent on the best fit rectangular fault planes. Such discrepancies further indicate that strike and dip variations on the faults can modulate the direction of fault slip. Our observation agrees with previous investigations of the relationship between fault geometry and induced stress. Model experiments on post-glacial unloading from Hampel et al. (2010) suggested that fault dip could control the duration and timing of the slip accumulation phase and the magnitude of slip rate variations. Recently, Li et al. (2020) suggest that the surface mass distribution induced stress calculated on fault planes can be quite sensitive to the assumed fault geometry, and especially the dip angle. Notably, our modeled results on stress and slip show an accumulative amplitude change over 150 kyr, with the assumption that there are no major ruptures that change this fault geometry. Therefore, paleoearthquakes within the past 150 kyr and their energy release and changes on fault geometry could influence the

The influence of the Earth material properties on the results can be considerable, therefore we develop experiments with three different Earth structures (Fig. S2) on SBF. Earth structure 1 (the primary Earth property use applied in the stress/slip calculation) represents a lower viscosity of lithospheric mantle, than that of

Earth structure 2 (Fig. S2), and the Earth structure 3 presents the case with weak lower crust. The results from this experiment show that the slip patterns of these three Earth structures are the same; however, we found that viscosity can modulate the magnitude of the slip on the fault plane (Fig. S5). For a weak lithospheric mantle (Earth structure 1), the loading induced slip is more pronounced than that of Earth structure 2, and the difference of accumulated slip between these two Earth structures can be ~ 1 m (Fig. S5). Meanwhile, a weak lower crust would result in a higher accumulated slip (\sim 0.5 m) on fault planes. Moreover, we also observe along-strike heterogeneity on the slip rate, where the north tip of fault has more slip change than that from the south. Such influence of Earth structure on loading-induced slip is also supported by numerical experiments on glacier-induced slip, where slip rate of normal faults would be less pronounced when lower crustal viscosity increases (Hampel et al., 2010). Steffen et al. (2014) also noted that the Earth material parameters, including the thickness of crust and lithosphere, are major parameters affecting the modeled magnitude of ice-sheet melting induced fault slip. This comparison suggests that the magnitude of the reduction of the slip rate caused by lake loading is also affected by changing the viscosity of the lithospheric mantle, especially in the EAR where rift location and initial evolution have been controlled by lithosphericscale pre-existing crust and mantle heterogeneity.

In addition to the elastic loading of water storage on the surface, pore pressure changes can also play an important role in Coulomb stress calculation for fault interaction studies (e.g., Sumy et al., 2014). Here, we demonstrate the potential influence of pore fluid pressure on the stress changes of fault planes. The pore fluid pressure change of undrained loading is given by $\Delta p = -B \Delta \sigma_{kk}/3$, where $\Delta\sigma$ is the change in stress tensor and B is the Skempton coefficient (e.g., Rice and Cleary, 1976) in the range of 0.5 and 0.9, based on a compilation of experiments (Roeloffs, 1996). We apply a B of 0.7 and stress tensor changes from lake water storage, and calculate the pore pressure and Coulomb stress using $\Delta CFS = \Delta \tau - \mu(\Delta \sigma_n + \Delta p)$ on the three points along the SBF would promote the pore fluid pressure, and further increase the effective normal stress on the fault plane (Fig. S6). The magnitude of modeled Coulomb stress is reduced 20-32%, considering such an increase in effective normal stress. Clearly, significant uncertainties remain in these estimates of pore fluid pressure, and a better approach would require further constraints on the reservoir shape and physical properties, i.e. the porosity, compressibility, drained situation, and poroelastic properties. Although we cannot directly quantify the pore fluid pressure in absence of constraining evidence, the modeled results presented here are only an example of the potential influence of lake level change-induced pore fluid pressure on effective normal stress on the fault planes. Additionally, the stress is also dependent on the fault depth. We focus on the fault plane at a depth of 10 km due to the limits of seismic reflection studies (Scholz et al., 2020). To investigate the influence of fault depth on the stress, we assume a flat plane and project stress tensors on a fault plane with the geometry of strike = 0, dip = 60, and rake = 90 (Fig. S7). We calculate the time series of Coulomb stress at the location of SBF (x = 644 km and y = 8811 km) and cells at different depths (2, 6, 11, 27 km). The result shows that rift lake loading-derived stress decreases with depth and it reduces 81% in the lower crust with the assumed fault geometry, suggesting the rift lake-derived stress change likely has the most effect on faults within upper crust.

Our models have some inherent limitations. We acknowledge that this approach does not take into account some factors that modified the stress and slip rate on the rift fault planes, including the influence of other intrarift faults in the Central Basin (see Fig. 1b), the primary border faults to the west, and the partial overlapping of target faults along the rift axis. These factors may also

contribute to the total extension rate and strain localization and further impact the modeled stress and slip on the faults. Using only three faults in the model may underestimate the contribution from other faults in the Central Basin. Note however that the model focuses on the elastic properties of the Earth materials. Regional and local flexural uplift in response to the rift lake unloading is not explored in this work, which may also generate some differences and influence fault offsets and patterns of fault migration.

6. Conclusions

Three-dimensional finite element modeling of faults enables evaluating the spatiotemporal evolution of transient stress changes and slip rate variations on border and intrarift faults in the Lake Malawi Rift over the past 150 kyr. Our results suggest the following broad set of conclusions:

- (1) Lake water column fluctuations of ~600 m exert as much as 0.9 MPa shear stress and 4.6 MPa normal stress on fault planes over the studied interval of the late-Quaternary. Such stress change magnitudes are sufficient to influence fault rupture and associated earthquakes.
- (2) An increase in lake level produces a negative Coulomb stress on fault planes and gives rise to fault clamping and reduction in fault slip in extensional settings. Our modeling results agree with previous studies that focused on the effect of glacial loading/unloading cycles on fault activity. Reconstructing water column loading histories of active faults by using continental paleoclimate archives can help better understand past and future strain release patterns of seismogenic faults.
- (3) The magnitude of stress and slip changes on individual faults also vary (~1 MPa Coulomb stress and 2 m of slip) along strike due to variable fault geometries and position relative to the center of the water column load. This stress variation along fault strike may explain the different strain accommodated on the intrarift faults along the Malawi Rift.
- (4) Assumed Earth model parameters and pore fluid pressure also influence fault throw and stress changes on fault planes. For example, a weak lithospheric mantle versus a strong one would produce a slip difference of 2 m on the faults.

In summary, our results highlight the rich interplay between tectonics and climate and between the earthquake cycle and climate cycle, which indicate long-term climate driven surface mass changes, including hydro-loading, can modulate active deformation patterns and fault behaviors in continental rifts. Rift lakes with similar characteristics along the EAR may have experienced comparable tectonic-climate interactions during Pleistocene and Holocene.

CRediT authorship contribution statement

Liang Xue: Investigation, Methodology, Writing – original draft. **Robert Moucha:** Methodology, Writing – review & editing. **Christopher A. Scholz:** Project administration, Validation, Writing – review & editing.

Declaration of competing interest

The authors declare that they have no known competing financial interests or personal relationships that could have appeared to influence the work reported in this paper.

Acknowledgements

We thank two anonymous reviewers and the Associate Editor for providing constructive reviews of an earlier version of the manuscript. Support for studies of rift-climate interactions is provided by Chevron and Petrobras to Syracuse University. Partial support for LX comes from the Office of Research at Syracuse University. LX thanks the Computational Infrastructure for Geodynamics (CIG) PyLith group for providing workshops and forum on PyLith. The PyLith code (Aagaard et al., 2013) can be obtained at CIG (geodynamics.org/cig/software/pylith/). The PyLith model input (configuration) parameters are uploaded in the Open Science Framework depository (DOI: https://doi.org/10.17605/OSF.IO/ UNBK8). The quantitative lake level history of Lake Malawi is available at the NOAA archive (https://www.ncei.noaa.gov/access/paleosearch/study/19424) and in the OSF archive. Bathymetric data from Lake Malawi are uploaded into the Marine Geoscience Data System (Data DOI: https://doi.org/10.26022/IEDA/330928).

Appendix A. Supplementary material

Supplementary material related to this article can be found online at https://doi.org/10.1016/j.epsl.2022.117693.

References

- Aagaard, B., Knepley, M., Williams, C., 2017. PyLith v2. 2.1, Computational infrastructure for geodynamics. Zenodo.
- Aagaard, B.T., Knepley, M.G., Williams, C.A., 2013. A domain decomposition approach to implementing fault slip in finite-element models of quasi-static and dynamic crustal deformation. J. Geophys. Res., Solid Earth 118 (6), 3059–3079.
- Albaric, J., Déverchère, J., Petit, C., Perrot, J., Le Gall, B., 2009. Crustal rheology and depth distribution of earthquakes: insights from the central and southern East African rift system. Tectonophysics 468 (1–4), 28–41.
- Andrews, D.J., 2005. Rupture dynamics with energy loss outside the slip zone. J. Geophys. Res., Solid Earth 110 (B1).
- Ballato, P., Brune, S., Strecker, M.R., 2019. Sedimentary loading-unloading cycles and faulting in intermontane basins: insights from numerical modeling and field observations in the NW Argentine Andes. Earth Planet. Sci. Lett. 506, 388–396.
- Bettinelli, P., Avouac, J.P., Flouzat, M., Bollinger, L., Ramillien, G., Rajaure, S., Sapkota, S., 2008. Seasonal variations of seismicity and geodetic strain in the Himalaya induced by surface hydrology. Earth Planet. Sci. Lett. 266 (3–4), 332–344.
- Bootsma, H., Hecky, R.J.S.G., 1999. Water Quality Report, Lake Malawi/Nyasa Biodiversity Conservation Project.
- Borsa, A.A., Agnew, D.C., Cayan, D.R., 2014. Ongoing drought-induced uplift in the western United States. Science 345 (6204), 1587–1590.
- Calais, E., Freed, A.M., Van Arsdale, R., Stein, S., 2010. Triggering of new Madrid seismicity by late-Pleistocene erosion. Nature 466 (7306), 608-611.
- Clement, A.C., Hall, A., Broccoli, A.J., 2004. The importance of precessional signals in the tropical climate. Clim. Dyn. 22 (4), 327–341.
- Craig, T.J., Calais, E., Fleitout, L., Bollinger, L., Scotti, O., 2016. Evidence for the release of long-term tectonic strain stored in continental interiors through intraplate earthquakes. Geophys. Res. Lett. 43 (13), 6826–6836.
- Delvaux, D., Barth, A., 2010. African stress pattern from formal inversion of focal mechanism data. Tectonophysics 482 (1–4), 105–128.
- Drayton, R.S., 1984. Variations in the level of Lake Malawi. Hydrol. Sci. J. 29 (1), 1–12.
- Dziewonski, A.M., Anderson, D.L., 1981. Preliminary reference Earth model. Phys. Earth Planet. Inter. 25 (4), 297–356.
- Ebinger, C.J., Rosendahl, B.R., Reynolds, D.J., 1987. Tectonic model of the Malaŵi rift, Africa. Tectonophysics 141 (1–3), 215–235.
- Hampel, A., Hetzel, R., 2006. Response of normal faults to glacial-interglacial fluctuations of ice and water masses on Earth's surface. J. Geophys. Res., Solid Earth 111 (B6).
- Hampel, A., Hetzel, R., Densmore, A.L., 2007. Postglacial slip-rate increase on the Teton normal fault, northern basin and range province, caused by melting of the Yellowstone ice cap and deglaciation of the Teton Range? Geology 35 (12), 1107–1110.
- Hampel, A., Karow, T., Maniatis, G., Hetzel, R., 2010. Slip rate variations on faults during glacial loading and post-glacial unloading: implications for the viscosity structure of the lithosphere. J. Geol. Soc. 167 (2), 385–399.
- Hodge, M., Biggs, J., Fagereng, Å., Mdala, H., Wedmore, L.N.J., Williams, J.N., 2020. Evidence from high-resolution topography for multiple earthquakes on high slip-to-length fault scarps: the Bilila-Mtakataka fault, Malawi. Tectonics 39 (2), e2019TC005933.

- Johnson, C.W., Fu, Y., Bürgmann, R., 2017. Seasonal water storage, stress modulation, and California seismicity. Science 356 (6343), 1161–1164.
- King, G.C., Stein, R.S., Lin, J., 1994. Static stress changes and the triggering of earth-quakes. Bull. Seismol. Soc. Am. 84 (3), 935–953.
- Kolawole, F., Atekwana, E.A., Laó-Dávila, D.A., Abdelsalam, M.G., Chindandali, P.R., Salima, J., Kalindekafe, L., 2018. Active deformation of Malawi rift's North basin Hinge zone modulated by reactivation of preexisting Precambrian Shear zone fabric. Tectonics 37 (3), 683–704.
- Laó-Dávila, D.A., Al-Salmi, H.S., Abdelsalam, M.G., Atekwana, E.A., 2015. Hierarchical segmentation of the Malawi Rift: the influence of inherited lithospheric heterogeneity and kinematics in the evolution of continental rifts. Tectonics 34 (12), 2399–2417.
- Li, S., Wdowinski, S., Hsu, Y.J., Shyu, J.B.H., 2020. Earthquake interactions in central Taiwan: probing Coulomb stress effects due to ML ≥ 5.5 earthquakes from 1900 to 2017. J. Geophys. Res., Solid Earth 125 (8), e2019]B019010.
- Lyons, R.P., Scholz, C.A., Buoniconti, M.R., Martin, M.R., 2011. Late quaternary stratigraphic analysis of the Lake Malawi Rift, East Africa: an integration of drill-core and seismic-reflection data. Palaeogeogr. Palaeoclimatol. Palaeoecol. 303 (1–4), 20–37.
- Lyons, R.P., Scholz, C.A., Cohen, A.S., King, J.W., Brown, E.T., Ivory, S.J., et al., 2015. Continuous 1.3-million-year record of East African hydroclimate, and implications for patterns of evolution and biodiversity. Proc. Natl. Acad. Sci. 112 (51), 15568–15573.
- McSweeney, C., New, M., Lizcano, G., 2014. UNDP climate change country profiles Malawi.
- Messager, M.L., Lehner, B., Grill, G., Nedeva, I., Schmitt, O., 2016. Estimating the volume and age of water stored in global lakes using a geo-statistical approach. Nat. Commun. 7 (1), 1–11.
- Mörner, N.A., 2005. An interpretation and catalogue of paleoseismicity in Sweden. Tectonophysics 408 (1–4), 265–307.
- Njinju, E.A., Atekwana, E.A., Stamps, D.S., Abdelsalam, M.G., Atekwana, E.A., Mickus, K.L., et al., 2019. Lithospheric structure of the Malawi Rift: implications for magma-poor rifting processes. Tectonics 38 (11), 3835–3853.
- Olive, J.A., Behn, M.D., Malatesta, L.C., 2014. Modes of extensional faulting controlled by surface processes. Geophys. Res. Lett. 41 (19), 6725–6733.
- Rice, J.R., Cleary, M.P., 1976. Some basic stress diffusion solutions for fluid-saturated elastic porous media with compressible constituents. Rev. Geophys. 14 (2), 227–241.
- Roeloffs, E., 1996. Poroelastic techniques in the study of earthquake-related hydrologic phenomena. Adv. Geophys. 37, 135–195.
- Saria, E., Calais, E., Stamps, D.S., Delvaux, D., Hartnady, C.J.H., 2014. Present-day kinematics of the East African Rift. J. Geophys. Res., Solid Earth 119 (4), 3584–3600.
- Scholz, C.A., Cohen, A.S., Johnson, T.C., King, J., Talbot, M.R., Brown, E.T., 2011. Scientific drilling in the Great Rift valley: the 2005 Lake Malawi scientific drilling project—an overview of the past 145,000 years of climate variability in Southern Hemisphere East Africa. Palaeogeogr. Palaeoclimatol. Palaeoecol. 303 (1–4), 3–19.
- Scholz, C.A., Johnson, T.C., Cohen, A.S., King, J.W., Peck, J.A., Overpeck, J.T., et al., 2007. East African megadroughts between 135 and 75 thousand years ago and bearing on early-modern human origins. Proc. Natl. Acad. Sci. 104 (42), 16416–16421.
- Scholz, C.A., Shillington, D.J., Wright, L.J., Accardo, N., Gaherty, J.B., Chindandali, P., 2020. Intrarift fault fabric, segmentation, and basin evolution of the Lake Malawi (Nyasa) Rift, East Africa. Geosphere 16 (5), 1293–1311.
- Shillington, D.J., Scholz, C.A., Chindandali, P.R., Gaherty, J.B., Accardo, N.J., Onyango, E., et al., 2020. Controls on Rift faulting in the North Basin of the Malawi (Nyasa) Rift, East Africa. Tectonics 39 (3), e2019TC005633.
- Stamps, D.S., Calais, E., Saria, E., Hartnady, C., Nocquet, J.M., Ebinger, C.J., Fernandes, R.M., 2008. A kinematic model for the East African Rift. Geophys. Res. Lett. 35 (5).
- Stamps, D.S., Saria, E., Kreemer, C., 2018. A geodetic strain rate model for the East African Rift system. Sci. Rep. 8 (1), 1–9.
- Steer, P., Simoes, M., Cattin, R., Shyu, J.B.H., 2014. Erosion influences the seismicity of active thrust faults. Nat. Commun. 5 (1), 1–7.
- Steffen, R., Wu, P., Steffen, H., Eaton, D.W., 2014. The effect of Earth rheology and ice-sheet size on fault slip and magnitude of postglacial earthquakes. Earth Planet. Sci. Lett. 388, 71–80.
- Sumy, D.F., Cochran, E.S., Keranen, K.M., Wei, M., Abers, G.A., 2014. Observations of static Coulomb stress triggering of the November 2011 M5. 7 Oklahoma earthquake sequence. J. Geophys. Res., Solid Earth 119 (3), 1904–1923.
- Sun, M., Gao, S.S., Liu, K.H., Mickus, K., Fu, X., Yu, Y., 2021. Receiver function investigation of crustal structure in the Malawi and luangwa rift zones and adjacent areas. Gondwana Res. 89, 168–176.
- Thatcher, W., 1984. The earthquake deformation cycle, recurrence, and the time-predictable model. J. Geophys. Res., Solid Earth 89 (B7), 5674–5680.
- Tierney, J.E., Russell, J.M., Huang, Y., Damsté, J.S.S., Hopmans, E.C., Cohen, A.S., 2008. Northern hemisphere controls on tropical southeast African climate during the past 60,000 years. Science 322 (5899), 252–255.
- Ustaszewski, M.E., Pfiffner, O.A., 2008. Composite faults in the Swiss Alps formed by the interplay of tectonics, gravitation and postglacial rebound: an integrated field and modelling study. Swiss J. Geosci. 101 (1), 223–235.

- Wedmore, L.N., Biggs, J., Floyd, M., Fagereng, Å., Mdala, H., Chindandali, P., et al., 2021. Geodetic constraints on cratonic microplates and broad strain during rifting of thick Southern African lithosphere. Geophys. Res. Lett. 48 (17), e2021GL093785.
- Williams, J.N., Wedmore, L.N., Scholz, C.A., Kolawole, F., Wright, L.J., Shillington, D., et al., 2021. The Malawi active fault database: an onshore-offshore database for regional assessment of seismic hazard and tectonic evolution. Earth Space Sci. Open Arch. ESSOAr.
- Wu, P., Hasegawa, H.S., 1996. Induced stresses and fault potential in eastern Canada due to a disc load: a preliminary analysis. Geophys. J. Int. 125 (2), 415–430. Xue, L., Johnson, C.W., Fu, Y., Bürgmann, R., 2020. Seasonal seismicity in the
- Xue, L., Johnson, C.W., Fu, Y., Bürgmann, R., 2020. Seasonal seismicity in the western branch of the East African rift system. Geophys. Res. Lett. 47 (6), e2019GL085882.